Genotype–structure–phenotype correlations define divergent natural history in early-onset spastic paraplegia type 4

Julian E. Alecu,[1,2,3] Luca M. Schierbaum,[1] Amy Tam,[1] Vicente Quiroz,[1] Katerina Bernardi,[1] Kathryn Yang,[1] Johanna R. Roller,[2,3] Marion Döbler-Neumann,[4] Tim W. Rattay,[2,3,5] Carelis González-Salazar,[6] Elena A. Zehr,[7] Daniils Skorohodovs,[1] Josh Rong,[1] Siofra Carty,[1] Nicole Battaglia,[1] Seungbok Lee,[8,9] Jangsup Moon,[8,9] Michelle Christie,[10,11] Antonina Roll-Mecak,[7] Marcondes C. França Jr,[6] Rebecca Schüle,[12] Ludger J. Schöls[2,3] and Darius Ebrahimi-Fakhari[1,13]

Abstract

Hereditary spastic paraplegia type 4 (SPG4), caused by variants in *SPAST*, is the most common form of HSP and exhibits a remarkable phenotypic heterogeneity ranging from late-onset pure presentations to severe, early-onset complex disease. Robust genotype–phenotype correlations and detailed natural history data are lacking, limiting clinical trial readiness.

We analyzed 206 patients with genetically confirmed SPG4 enrolled across seven international centers, complemented by high-quality literature-derived cases. Deep phenotyping included standardized motor scales, spasticity ratings, developmental milestones, and patient-reported outcomes. We developed an extended essentiality-mapping framework to classify *SPAST* missense variants by integrating *in silico* pathogenicity predictions, evolutionary constraint, physicochemical residue connectivity, and variant enrichment within the human spastin hexamer structure. Plasma neurofilament light chain (pNfL) using was quantified using Simoa in 26 patients and 101 controls.

We identified 136 distinct *SPAST* variants, including 10 novel variants. Variant class segregated strongly by inheritance, with *de novo* cases enriched for missense variants and inherited cases showing a variety of variant classes with enrichment for truncating variants. Longitudinal analysis revealed two latent trajectories: a rapidly progressive severe subgroup enriched for *de novo* missense variants, and a biphasic moderate subgroup enriched for inherited truncating variants. Patient stratification integrating spastin essentiality mapping (missense variants affecting essential, neutral, or context-dependent

residues) with established genetic modifiers (biallelic pathogenic variants or modifier variants *in trans*) classified patients into predicted severe and moderate subgroups with divergent age at onset and clinical disease progression. The severe subgroup showed early developmental delays, rapid loss of ambulation, and declining quality of life, while the moderate subgroup displayed delayed but accelerating disease progression. pNfL levels were elevated in both subgroups, most pronounced in severe early disease.

This study provides the most detailed natural history of SPG4 to date and introduces a biologically informed stratification framework that links variant class and location to divergent clinical trajectories. These data establish clinically meaningful benchmarks and offer a genotype-based framework to improve anticipatory care and optimize trial design for SPG4.

Author affiliations:

1 Movement Disorders Program, Department of Neurology and F.M. Kirby Neurobiology Center, Boston Children's Hospital, Harvard Medical School, Boston 02115, MA, USA

2 Department of Neurodegenerative Diseases, Hertie-Institute for Clinical Brain Research, and Center of Neurology, University of Tübingen, 72076 Tübingen, Germany

3 German Center of Neurodegenerative Diseases (DZNE), 72076 Tübingen, Germany

4 Department of Pediatric Neurology, University Children's Hospital, 72076 Tübingen, Germany

5 Department of Neurology and Center for Rare Neurological Diseases (ZSNE), University Hospital Schleswig-Holstein (UKSH), Campus Kiel, 24105 Kiel, Germany

6 Department of Neurology, University of Campinas (UNICAMP), Campinas, São Paulo, 13083-970, Brazil

7 Cell Biology and Biophysics Unit, National Institute of Neurological Disorders and Stroke, Bethesda, MD 20892, USA

8 Department of Neurology, Seoul National University, Seoul, 03080, South Korea

9 Department of Genomic Medicine, Seoul National University, Seoul, 03080, South Korea

10 Department of Neurology and Rehabilitation Medicine, Texas Scottish Rite Hospital, University of Texas Southwestern Medical Center, Dallas, TX 75219, USA

11 Spastic Paraplegia - Centers of Excellence Research Network (SP-CERN), Dallas, TX 75219, USA

12 Division of Neurodegenerative Diseases and Movement Disorders, Department of Neurology, Heidelberg University Hospital and Faculty of Medicine, 69120 Heidelberg, Germany

13 Spastic Paraplegia - Centers of Excellence Research Network (SP-CERN), Boston 02115, MA, USA

Correspondence: Dr Darius Ebrahimi-Fakhari

Movement Disorders Program

Department of Neurology, Boston Children's Hospital

300 Longwood Avenue, Boston, MA 02215, USA

E-mail: darius.ebrahimi-fakhari@childrens.harvard.edu

Running title: Natural history of early-onset SPG4

Keywords: spastic paraplegia, spg4, natural history, SPAST, genotype-phenotype correlation, clinical trial readiness

ORCID iDs

Julian E. Alecu	0000-0002-1420-9775
Amy Tam	0000-0003-2072-3436
Vicente Quiroz	0009-0005-9212-0943
Katerina Bernardi	0009-0004-3387-7623
Kathryn Yang	0009-0004-6892-5189
Johanna R. Roller	0009-0006-9751-4180
Tim W. Rattay	0000-0002-5456-7761
Carelis González-Salazar	0000-0003-2300-682X
Elena A. Zehr	0000-0002-9768-5792
Nicole Battaglia	0009-0008-9751-4580
Jangsup Moon	0000-0003-1282-4528
Seungbok Lee	0000-0002-6620-6269
Michelle Christie	0000-0002-1329-8008
Antonina Roll-Mecak	0000-0003-2621-7307

Marcondes C. França Jr 0000-0003-0898-2419
Rebecca Schüle 0000-0002-7781-2766
Ludger Schöls 0000-0001-7774-5025
Darius Ebrahimi-Fakhari 0000-0002-0026-4714

Introduction

The hereditary spastic paraplegias (HSP) are an evolving group of over 90 monogenic disorders that primarily affect corticospinal motor neurons[1-3] and collectively represent the most common cause of inherited spasticity and associated disability worldwide[4-6].

Spastic paraplegia type 4 (SPG4, HSP-*SPAST*, OMIM #182601) is the most prevalent HSP subtype across diverse populations, accounting for 22% to 41% of HSP cases[7-13]. Heterozygous variants in *SPAST* cause SPG4, although a small number of patients with biallelic variants have also been reported. Both autosomal dominant inheritance and *de novo* occurrence are observed, with *SPAST* variants accounting for the majority of autosomal dominant[7,14-16] and approximately one-fifth of all *de novo* HSP cases[17,18].

SPAST encodes the AAA (ATPases Associated with diverse cellular Activities) ATPase spastin. Alternative translation initiation generates two major isoforms with distinct functions[19]. M87-spastin, translated from the second start codon and lacking the N-terminal hydrophobic domain[20,21], forms homohexameric complexes that act as microtubule (MT) severing enzymes [22-27], governing the balance of MT depolymerization and regrowth[28,29], essential for numerous cellular processes. Both the MT-binding and AAA ATPase domain are indispensable for severing: spastin engages the polyglutamylated C-terminus of β-tubulin[30] within the hexamer's pore formed by the AAA ATPase domains, and ATP hydrolysis drives MT lattice disruption[24,26,27]. Depending on cellular context, severing can lead to microtubule depolymerization or microtubule amplification by generating new seeds for microtubule polymerization and promoting lattice repair[28,29]. This is essential for cortical neuron development and survival, where intact MT dynamics are prerequisite for the morphogenesis and maintenance of long projecting axons[31-36]. By contrast, M1-spastin has broader context-dependent roles, including regulation of endoplasmic reticulum (ER) morphology, ER–organelle contact sites, Ca^{2+} signaling, endosomal trafficking, and lipid-droplet biology[37-41]. Both isoforms are expressed in brain and spinal cord[25], but M1 levels are tightly regulated through restricted translation initiation[19,20] and targeted degradation[42-44], resulting in low abundance in the brain[25].

Clinically, SPG4 presents with remarkable heterogeneity despite classically being considered a rather pure form of HSP[45]. Phenotypes range from a complex infantile-onset

neurological syndrome with global developmental delay, seizures, and early spastic tetraparesis, to early-onset lower limb spastic paraparesis with mild or absent developmental impairments, to late-onset pure HSP, all following distinct patterns of disease progression[46-50]. Despite multiple efforts, robust genotype-phenotype correlations have not been established[46,48-51]. A notable exception is the severe early-onset phenotype associated with biallelic *SPAST* variants, either a pathogenic allele *in trans* with a non-pathogenic intragenic modifier such as p.(Ser44Leu), or two pathogenic variants[46,48,50,52,53].

To date, no detailed natural history characterization of SPG4 incorporating both clinician- and patient-reported outcome measures - critical for interventional trials - has been available. This gap poses a major barrier as emerging therapeutic strategies advance toward clinical testing[44,54-56]. Given the small cohorts typical of rare disease trials, biologically informed patient stratification and precise delineation of natural disease progression are essential to maximize statistical power and detect treatment effects within limited observational periods[57].

Here, we investigate genotype–phenotype correlations and the natural history of SPG4, with a focus on divergent clinical trajectories. To maximize sensitivity for detecting meaningful associations, we concentrated on the disease phase characterized by the greatest phenotypic variability. Prior studies have demonstrated substantial heterogeneity in age at onset and clinical presentation during childhood, adolescence, and early adulthood, including a bimodal distribution of onset with peaks in childhood and the third to fourth decade of life, evidence of prodromal and often subclinical pathological changes in *SPAST* variant carriers preceding clinical self-recognition, and reports of early-onset, severe phenotypes associated with specific variant classes. Accordingly, we enrolled individuals younger than 40 years of age with genetically confirmed SPG4 from seven academic centers across four continents, assembling a cohort of 206 patients with deep clinical phenotyping and outcome measures prioritized for natural history studies and future clinical trial design.

Materials and methods

Study design, cohort and clinical characterization

Patients were enrolled through the Registry and Natural History Study for Early-Onset Hereditary Spastic Paraplegia (NCT04712812; Boston Children's Hospital IRB: P00033016) with data contributed by seven collaborating centers across North America, South America, Europe, and Asia. The study was conducted in accordance with the Declaration

of Helsinki and received ethical approval at all participating sites. Inclusion criteria were: (i) a confirmed pathogenic or likely pathogenic *SPAST* variant, (ii) clinical signs of disease on neurological examination, and (iii) age ≤40 years. All participants were evaluated by board-certified neurologists with expertise in HSP using standardized examination protocols. Variant pathogenicity was determined according to ACMG criteria.

Clinical assessments included the Spastic Paraplegia Rating Scale (SPRS)[58], SPATAX-EUROSPA disability stage (SPATAX), Gross Motor Function Classification System (GMFCS), and the modified Ashworth Scale to evaluate tone in upper limbs (elbow, wrist, thumb, fingers) and lower limbs (quadriceps, hamstrings, gastrocnemius, soleus). The SPRS spasticity subscore was derived from items 7-10. Developmental quotients and motor milestone data were systematically collected. Patient-reported outcomes included the Caregiver Priorities and Child Health Index of Life with Disabilities (CPCHILD), a validated measure of health-related quality of life in children with neurodevelopmental disabilities. No post hoc score calibration across centers was performed.

In addition, a systematic literature review (Table S1) identified 146 previously described patients meeting the same inclusion criteria with high-quality patient-level data. These cases were included exclusively in analyses of genetic spectrum and disease progression using SPRS, SPATAX, and GMFCS. Literature-derived cases were included only if patient-level clinical scores or clearly defined motor milestones were explicitly reported and could be directly mapped to these instruments. Cases with ambiguous, aggregated, or non-comparable data were excluded. Missing data were handled in an analysis-specific manner, with patients contributing only to analyses for which the relevant variables were available. No imputation of missing data was performed.

The dataset included 21 individuals carrying biallelic *SPAST* configurations (five from the multicenter cohort and sixteen literature-derived cases), including patients with two pathogenic variants as well as individuals carrying a pathogenic variant *in trans* with the established modifier variants p.(Ser44Leu) or p.(Pro45Gln). These cases were retained in the analyses given the well-established association of such configurations with severe SPG4 phenotypes[48,50,52,53,59].

Essentiality mapping of spastin residues

To stratify *SPAST* missense variants by functional relevance, we adapted the Essential3D framework by Iqbal and Brünger et al. [60,61] which integrates evolutionary conservation, missense constraint, and pathogenic variant enrichment in spatial context to identify functionally essential protein regions.

We introduced three extensions: (i) composite pathogenicity scoring by integrating predictions from 14 *in silico* tools for all possible amino acid substitutions per residue, with the standard deviation across substitutions retained as a measure of context dependence; (ii) unified evolutionary conservation scoring from nine conservation metrics across multiple phylogenetic clades; and (iii) residue connectivity analysis using evolutionary coupling and physicochemical interaction networks to validate functional interdependence assumptions and reduce false positives in essential site identification. Three-dimensional burden analysis compared pathogenic variants (ClinVar, HGMD) versus population variants (gnomAD). Analyses were performed using the human wild-type spastin hexamer structure (PDB: 6PEN)[22]. A detailed description of spastin essentiality mapping is provided in the *Supplementary material, Methods*.

Neurofilament light Single-Molecule Array Measurements

Plasma neurofilament light (pNfL) levels were measured as previously described[62]. Briefly, plasma samples were obtained by standard venipuncture, and NfL measurements in duplicates using the Simoa HD-X Analyzer platform with the Simoa NF-light V2 Advantage Kit (Quanterix, Cat#104073). Further details are provided in the *Supplementary material, Methods*.

Statistical analysis

A full description of all statistical analyses is provided in the *Supplementary material, Methods*.

Results

Demographic characteristics of the prospective cohort

A total of 206 patients with SPG4 were enrolled from seven centers across the USA, Germany, Brazil, and South Korea. The cohort included 126 males (61.2%) and 80 females (38.8%). Median age at enrollment was 11.2 years (IQR 19.3), and median age at last follow-up was 12.9 years (IQR 20.6). Longitudinal data were available for 102 patients; 43 had ≥3 visits and 17 had ≥4 visits over a median interval of 15.6 months (IQR 14.4).

Molecular spectrum of early-onset SPG4

Across 206 patients, 136 distinct *SPAST* variants were identified, including ten not previously reported (Table S2). Missense variants predominated (45.3%), followed by deletions (16.1%), nonsense (13.1%), and splicing variants (13.1%) (Figure 1A). One patient carried a pathogenic exon gain variant encompassing duplicated exons 5-16.

Inheritance was determined in 183 patients (88.8%): 90 had *de novo* variants (43.9%) confirmed by trio testing, and 93 had inherited variants (44.9%). Parental samples were unavailable for 23 patients, precluding definitive determination of inheritance. Variant distributions differed by inheritance. Inherited cases showed the expected distribution of coding impacts with truncating variants most frequent (nonsense 23.6%, deletions 22.5%, frameshift 13.5%), followed by splicing (20.2%) and missense variants (19.1%). By contrast, *de novo* cases were strongly enriched for missense variants (95.3%), consistent with literature data (93.1% of reported cases, Figure S1).

Recurrent missense variants included p.(Arg499His) in 42 patients, p.(Met390Val) in 6 patients, p.(Arg499Cys) in 4 patients, and p.(Leu195Val) in 3 patients. Most missense variants (90.2%) localized to the AAA ATPase domain, whereas truncating variants were more evenly distributed (Figure 1B).

Five patients carried biallelic *SPAST* variants: Two with intragenic modifier variant p.(Ser44Leu) *in trans* with splicing variants, one patient with the same modifier variant *in trans* with a frameshift variant, one with biallelic pathogenic missense variants, and one with frameshift and splicing variants *in trans*.

Exploring genotype-phenotype associations

SPG4 demonstrates substantial phenotypic pleiotropy, posing challenges for trial design and interpretation. Establishing generalizable genotype–phenotype associations is therefore critical for effective patient stratification. Three observations motivated our exploration: 1) *de novo* variants are associated with severe, early-onset, and complex phenotypes[47,49], 2) *de novo* cases are strongly enriched for missense variants (confirmed here)[49], and 3) although missense variants are linked to earlier onset and complex features, prior studies have not consistently associated them with worse motor function[48].

Exploratory longitudinal analysis of the SPRS revealed two distinct longitudinal patterns (Figure 1C). A rapidly progressive subgroup reached SPRS scores exceeding 20 points before age 10 and approached the upper range of observed scores by the second to third decade. A second apparent subgroup showed slower early progression with SPRS scores

remaining below 15 before age 10 and typically reaching values of 10-20 by the fourth decade. The rapidly progressing subgroup was enriched for missense variants mostly occurring *de novo*, the more slowly progressing subgroup was enriched for inherited truncating variants, although relevant overlap existed across categories.

Among 95 distinct missense variants in the combined prospective and literature-derived dataset, only three were shared between *de novo* and inherited cases, indicating near-complete inheritance-based segregation (Figure 1D). This genetic divide supported the hypothesis that different variants – particularly different missense variants – exert distinct molecular effects on spastin function, potentially driving distinct clinical trajectories.

Classifications based solely on variant type or inheritance did not adequately predict severity in this or prior studies[21,46,48,50] (Figure 1C), prompting development of a biologically informed stratification approach.

Spastin essentiality mapping

To classify *SPAST* missense variants by functional relevance, we adapted the Essential3D framework[60,61], which integrates missense constraint, evolutionary conservation, and pathogenic variant enrichment in protein structural context to identify functionally essential residues. We introduced three extensions: First, we replaced single-metric missense tolerance with composite scores from 14 *in silico* pathogenicity prediction tools, generating average pathogenicity scores for all possible substitutions per residue while retaining variability as a context-dependence measure. Second, we integrated nine conservation metrics across phylogenetic depths into unified evolutionary constraint scores. Third, we incorporated residue connectivity analyses using evolutionary coupling and physicochemical interaction networks to validate functional interdependence assumptions of three-dimensional residue neighborhoods. This framework was chosen over other variant classification approaches because it integrates relevant complementary data in the specific three-dimensional context of the protein of interest, making it particularly well-suited for the interrogation of potential genotype-phenotype correlations.

Analyses used the human wild-type spastin hexamer structure (PDB: *6PEN*)[22] spanning parts of the MT-binding and the full AAA domain (residues 318-610) where most missense variants localize. Consensus classification proceeded hierarchically (Figure 1E): Residues with minimal connectivity ($Z \leq -2$) were excluded from 3D analysis; remaining residues were evaluated for pathogenic variant enrichment, then conservation and missense constraint. Residues enriched for pathogenic variants ($OR > 1$, $p_{adj.} < 0.05$) with increased conservation and missense constraint ($Z > 0$) were classified as Essential3D sites.

Residues not enriched ($p_{adj.} \geq 0.05$) or depleted (OR < 1, $p_{adj.} < 0.05$) of pathogenic variants were classified as neutral sites. Residues enriched for pathogenic variants but not meeting the conservation or missense constraint criteria were further evaluated for increased variability in pathogenicity predictions (Z > 0), with high-variability residues classified as context-dependent sites.

Of 292 residues, 2.4% were unsuitable due to minimal connectivity (mostly loop residues at hexamer edges). The remainder were classified as neutral (42.3%), Essential3D (29.4%), or context-dependent (25.9%). For the latter, all possible missense variants were classified as either severe (Z > 0) or moderate (Z ≤ 0) based on variant-specific pathogenicity predictions.

Essential3D sites are enriched for functionally relevant structural features

Essential3D residues were significantly enriched for functionally critical structural features (Figure 2A). Using manual annotations from *D. melanogaster* homologue studies[23,63] and automated annotations derived from residue interaction networks (RIN), Essential3D sites were significantly enriched for pore loop 1 (OR = Inf [95%-CI 4.4-Inf], $p_{adj.}$ = 1.0e-3) and pore loop 2 (OR = 18.1 [95%-CI 2.3-822.9], $p_{adj.}$ = 0.011) residues, mostly corresponding to microtubule-interacting sites (OR = Inf [95%-CI 2.3-Inf], $p_{adj.}$ = 0.019). Nucleotide/ligand binding residues were overrepresented (RIN-based: OR = 7.0 [95%-CI 2.5-23.0], $p_{adj.}$ = 5.3e-4), as were residues of the Walker B motif crucial for ATP hydrolysis[23,64-66] (OR = Inf [95%-CI 3.0-Inf], $p_{adj.}$ = 9.0e-3). Manually annotated nucleotide binding sites ($p_{adj.}$ = 0.056) and Walker A motif residues ($p_{adj.}$ = 0.060) showed nominal but not FDR-corrected significance. Residues at protomer interfaces, presumed to mediate hexamerization, were not enriched among essential sites.

Recurrent variants at Arg499 exemplify context-dependent essentiality

Essentiality mapping revealed that residue 499, the arginine finger crucial for ATP hydrolysis[23] and most commonly affected in our cohort, was classified as context-dependent, while other residues crucial for ATP hydrolysis Lys388 and Glu442 (part of the Walker A and B motifs) were Essential3D sites (Figure 2B). Given substantial clinical heterogeneity reported for Arg499 variants[50,67-71], we systematically explored severity subclassifications for all potential substitutions.

Variants p.(Arg499Pro), p.(Arg499Leu), and p.(Arg499His) were predicted context-dependent severe, while p.(Arg499Gly), p.(Arg499Cys), and p.(Arg499Ser) were moderate (Figure 2C). Proline substitutions were absent in our cohort and the literature; histidine, leucine, and cysteine substitutions occurred in our cohort, and glycine in prior reports.

Longitudinal SPRS analysis revealed complete separation between severity subgroups (Figure 2D). Patients with p.(Arg499Cys) had consistently lower scores, whereas p.(Arg499His) and p.(Arg499Leu) showed higher scores and rapid progression.

Given the paucity of individual SPRS or comparable clinical scores in published reports, we analyzed age at symptom onset as an orthogonal and consistently documented variable to confirm these trends. Combined data of 95 patients with Arg499 variants derived from the literature and our cohort revealed significant onset differences across substitutions ($p = 2.6e-10$). Moderate variants p.(Arg499Gly) (median = 22 years, $p_{adj.} = 0.01$) and p.(Arg499Cys) (median = 13.5 years, $p_{adj.} = 2.9e-10$) showed later onset than p.(Arg499His) (median = 11.5 months) (Figure 2E), with larger onset variability for p.(Arg499Cys) (IQR 28.5 years) versus p.(Arg499His) (IQR 9.0 months).

Across all missense variants, Essential3D and context-dependent sites were associated with earlier onset than neutral sites, and context-dependent moderate variants with later onset than severe variants ($p < 1e-16$) (Figure 2A).

Patient stratification integrates essentiality mapping with established genotype-phenotype correlations

Next, we stratified the entire combined cohort (n = 352: 206 study patients, 146 literature patients) by integrating the novel essentiality classification of missense variants with established genetic factors known to influence SPG4 severity: biallelic pathogenic *SPAST* variants and intragenic modifier variants *in trans*[48,50,53,59,72].

Two predicted phenotypic subgroups emerged (Figure 2B). The predicted severe subgroup (n = 134, 38.1%) included missense variants affecting Essential3D residues, context-dependent severe variants, and biallelic *SPAST* variants including modifiers p.(Ser44Leu) and p.(Pro45Gln). Consistent with established genotype–phenotype correlations in SPG4, individuals carrying biallelic *SPAST* variants were classified within the predicted severe subgroup based on their known association with severe clinical presentations, which in the present cohort closely paralleled the trajectories observed in patients with predicted severe monoallelic missense variants. The predicted moderate subgroup (n = 218, 61.9%)

comprised missense variants at neutral residues, context-dependent moderate variants, monoallelic truncating/splice variants, and variants with uncertain classification.

Quality of life is predicted by essentiality-based stratification

To test whether this stratification captured patient-relevant differences, we analyzed CPCHILD scores (128 observations) from 73 patients. The CPCHILD quantifies disease impact on health-related quality of life as perceived by affected families[73].

Linear mixed-effects modeling with age-by-subgroup interaction, adjusted for inheritance and sex, revealed significant trajectory differences between subgroups (age×subgroup interaction p = 0.025) (Figure 2C). Estimated marginal trend (EMT) contrast analysis revealed significantly different slopes between the two subgroups (p = 0.026). To interpret age effects given the significant interaction, separate models were fitted for each subgroup, yielding an annual decline of -0.77 points (p = 0.027, R_m^2 = 0.15) in the severe subgroup, while the moderate subgroup showed no significant change over time (p = 0.16) (Figure 2D).

Cross-sectional analysis using estimated marginal means (EMM) demonstrated significant differences at multiple timepoints (Figure 2C). While no difference was evident at age 3 years, the severe subgroup scored an estimated 12.7 points lower at age 5 years (p = 0.023), with differences persisting at ages 10 years (18.3 points, p = 4.1e-4) and 20 years (29.3 points, p = 7.0e-5). Estimates beyond age 20 should be interpreted cautiously due to sparse data.

Clinical phenotypes diverge between subgroups

Firth's penalized logistic regression adjusted for inheritance, sex, and age revealed the severe subgroup had significantly increased odds for complex features extending well beyond “pure” HSP (Figure 2E).

Motor dysfunction was more pronounced, with increased odds for walking aid (OR = 19.4 [95%-CI 7.7-48.9], $p_{adj.}$ = 2.0e-8) and wheelchair dependence (OR = 27.1 [95%-CI 9.9-74.5], $p_{adj.}$ = 1.8e-8). Upper limb involvement included spasticity (OR = 611.5 [95%-CI 6.0-Inf], $p_{adj.}$ = 0.046) and weakness (OR = 27.1 [95%-CI 3.2-229.6], $p_{adj.}$ = 0.024). Secondary musculoskeletal manifestations including contractures of the lower limbs (OR = 6.7 [95%-CI 2.2-20.0], $p_{adj.}$ = 0.011), as well as muscle wasting (OR = 6.8 [95%-CI 2.2-21.1], $p_{adj.}$ = 0.011) were also more frequent. Neonatal/infantile hypotonia (OR = 8.2 [95%-CI 2.4-28.6],

$p_{adj.}$ = 0.011) typically progressed to hypertonia (OR = 9.5 [95%-CI 2.6-34.4], $p_{adj.}$ = 0.011). Neurodevelopmental abnormalities included speech delay (OR = 5.2 [95%-CI 1.7-16.2], $p_{adj.}$ = 0.037) and developmental regression (OR = 20.5 [95%-CI 4.5-92.3], $p_{adj.}$ = 2.7e-3). Additional manifestations encompassed urinary incontinence (OR = 4.5 [95%-CI 1.5-13.2], $p_{adj.}$ = 0.047), dysarthria (OR = 33.0 [95%-CI 3.0-364.3], $p_{adj.}$ = 0.037), history of aspiration (OR = Inf [95%-CI 157.5-Inf], $p_{adj.}$ = 0.041), and drooling (OR = 8.9 [95%-CI 1.9-43.3], $p_{adj.}$ = 0.046). Additional nominally significant associations not surviving FDR correction included intellectual disability (OR = 6.2, p = 0.028), developmental delay (OR = 7.9, p = 9.6e-3), dysphagia (OR = 14.7, p = 0.028), and non-verbal status (OR = 14.3, p = 0.018).

The moderate subgroup was more likely to achieve motor milestones, with higher odds for unsupported standing (OR = 14.3 [95%-CI 2.7-100.0], $p_{adj.}$ = 0.016) and walking (OR = 20.0 [95%-CI 5.9-100.0], $p_{adj.}$ = 4.6e-5).

Despite the conservative statistical approach that penalizes quasi-complete or complete separation yielding non-significant results for these findings, extrapyramidal movement disorders showed a clear pattern of subgroup specificity (Figure 2F). Both dystonia (19.3%) and parkinsonism (hypokinesia: 4.8%, rigidity: 3.6%) were exclusively observed in the severe subgroup.

Divergent motor functional progression

We evaluated the progression of functional motor impairment using SPATAX (451 observations, 251 patients) and GMFCS (273 observations, 132 patients) with survival and proportional-hazards analyses (Figure 3 & Supplementary Fig. S4).

Kaplan-Meier analysis revealed distinct progression patterns. The moderate subgroup declined gradually, losing running (SPATAX ≥3) at median 34.7 years and requiring walking aids (SPATAX ≥4) at 40 years; the severe subgroup reached these stages at 4 and 5 years, respectively (Figures 4a-b). Wheelchair dependence (SPATAX ≥6) occurred in 12.2% of moderate patients during observation versus 97.5% of severe patients at median 7.4 years. GMFCS results were concordant: Assistive mobility devices (≥III) were required at median 8.2 years in the severe subgroup versus 36.8 years in the moderate subgroup (Figure 4D and E).

Cox proportional hazards models adjusted for sex and inheritance confirmed relevant subgroup effects (Figure 4G-I). For SPATAX progression to walking aid (≥4) and wheelchair dependence (≥6), the severe subgroup showed 20.9-fold (HR = 20.89 [95%-CI 10.12-43.12], p = 2.1e-16) and 43.5-fold (HR = 43.46 [95%-CI 15.85-119.17], p = 2.3e-13) increased

hazards. For GMFCS progression to requiring an assistive mobility device (≥III) and severe mobility limitation (≥IV), hazard ratios were 17.8-fold (HR = 17.77 [95%-CI 4.85-65.13], p = 1.4e-5) and 27.1-fold (HR = 27.08 [95%-CI 5.39-136.03], p = 6.2e-5).

Both scales inversely correlated with quality of life: each one-point increase in SPATAX and GMFCS corresponded to 5.9- (p = 2.7e-4) and 6.5-point (p = 1.4e-6) decreases in CPCHILD (Figure 4C and F).

Progression of spasticity differs by subgroup

To characterize spasticity progression, we analyzed SPRS total scores and spasticity subscores using longitudinal mixed-effects modeling (Figure 5). Generalized additive mixed models revealed distinct age-score relationships between subgroups for both SPRS total and spasticity subscores. The moderate subgroup exhibited non-linearity (EDF = 2.54) for total scores, while the severe subgroup showed linear relationships. Automated breakpoint detection identified an inflection point at 13.7 years (95%-CI 8.9-18.5) for the moderate subgroup, which was incorporated into all subsequent analyses.

Linear mixed-effects models with age-by-subgroup interactions revealed significant trajectory differences. For SPRS total scores (444 observations, 271 patients), the interaction was significant (p = 5.1e-3) with different pre-breakpoint slopes (p = 2.5e-3) but convergent post-breakpoint progression (p = 0.26). Subgroup-specific modeling showed the severe subgroup had a consistent annual progression of +0.43 points (p = 4.7e-5, R_m^2 = 0.1), while the moderate subgroup exhibited biphasic progression: minimal pre-breakpoint change (p = 0.18) followed by acceleration after 13.7 years (+0.4 points/year, p = 6.7e-3, R_m^2 = 0.14).

Cross-sectional differences were substantial, with the severe subgroup scoring an estimated 19.4 points higher at age 3 (p = 5.9e-13), 23.1 points at age 7 (p = 1.3e-26), and stabilizing around 28.1 points at age 20 (p = 1.1e-34).

SPRS spasticity subscore analysis (338 observations, 177 patients) confirmed these patterns with significant interaction (p = 2.8e-8) and slope differences (p = 1.6e-8). Annual progression rates were +0.27 (p = 1.2e-11, R_m^2 = 0.34) and +0.04 points (p = 7.8e-3, R_m^2 = 0.1) in severe and moderate subgroups, respectively. Although non-linearity testing did not support delayed acceleration for the moderate subgroup's spasticity subscore, limited data may account for this and the overall small slope; applying the 13.7-year breakpoint did not improve fit.

Importantly, both measures correlated with declining quality-of-life, with each one-point increase decreasing CPCHILD scores by 0.94 (p = 4.7e-9) and 2.66 points (p = 2.2e-6) for total and spasticity subscores (Figure 5C and F).

Given prominent upper limb involvement in the severe subgroup (Figure 3E), we further examined spasticity in this subgroup using the modified Ashworth Scale (Figure 5G-H). Ordinal, non-linear mixed-effects modeling revealed a temporal gradient in the lower limbs: distal muscles showed higher initial grades (2) than proximal muscles (1/+1), with both reaching grade 3 by age 20 and grade 4 by age 30. Upper-limb spasticity emerged later (grade 1/1+ in the second decade) and accelerated in the third decade, typically reaching grades 2 and 3 at ~25 and ~30 years, respectively.

Anchor-based estimation of clinically important SPRS change

To define clinically meaningful SPRS change thresholds for interventional trials, we estimated minimal clinically important differences (MCID) anchored to the Clinical Global Impression-Improvement (CGI-C) scale using longitudinal data from 81 patients (Figure 5I). We evaluated six anchor categories reflecting varying levels of clinician-reported global change. For clinical improvement, any perceived improvement (CGI-C ≤ 3) corresponded to an estimated SPRS change of -4.51 points (95%-CI -6.67–-2.34; p = 1.2e-4; mean change = -2.1), while minimal improvement (CGI-C = 3) required -3.94 points (95%-CI -6.35–1.53; p = 2.0e-3; mean change = -1.8). For clinical worsening, any perceived deterioration (CGI-C ≥ 5) corresponded to +2.45 points (95%-CI 0.76-4.14; p = 6.0e-3; mean change = +2.3), while minimal worsening (CGI-C = 5) yielded +1.56 points but did not reach significance (95%-CI -0.23-3.35; p = 0.09; mean change = +2.0).

Severe subgroup presents with global developmental difficulties

Building on cross-sectional findings (Figure 3E), we analyzed motor milestone attainment and developmental quotients longitudinally. Kaplan-Meier analysis of gross motor milestones revealed substantial developmental delays in the severe subgroup (Figure 6A), with crawling achieved by 71.3% at median 14 months and walking with assistance by 77.4% at median 24 months. Subgroup comparisons showed significant differences for unsupported sitting (moderate: 100% at median 8 months vs. severe: 87.7% at median 9 months, p = 0.031, Figure S5), and more pronounced divergence for unsupported standing (moderate: 93.3% at median 14 months vs. severe: 40.1%, p = 3.2e-8, Figure 6B) and

walking (moderate: 91.3% at median 18 months vs. severe: 33.4%, p = 1.8e-12, Figure 6C). The moderate subgroup generally achieved milestones, albeit with modest delays.

Generalized additive mixed models for developmental quotients (DQ) suggested deviation from normal trajectories across domains (Figure 6D). Gross motor DQ started low and declined linearly; fine motor, expressive language, and social domains diverged during infancy/early childhood, deviated rapidly until ~8-10 years, then declined more slowly. Interpretation is, however, limited by small sample size.

Plasma neurofilament light is differentially elevated between subgroups

Blood NfL levels are moderately elevated in SPG4 with substantial variability[74-76] and limited data for younger patients. We measured plasma NfL (pNfL) using SiMoA in 26 SPG4 patients (median age: 10.4 years, IQR: 2.6–21.1; 46.7% female) and 101 age-matched controls (median age: 5.7 years, IQR: 0.6–24.8; 45.6% female), with longitudinal data available for four patients.

Generalized additive mixed modeling revealed distinct age-related trajectories (Figure 6E). The severe subgroup showed significant non-linear decrease over time (EDF = 1.89, p < 1e–16), the moderate subgroup linear progression (EDF = 1.00, p = 0.006), while controls showed minimal variation (EDF = 1.62, p = 0.18).

Cross-sectional differences were most pronounced at younger ages. At age 3, the severe subgroup had elevated estimated pNfL levels (59.8 pg/mL, 95%-CI 53.7–65.9) compared to the moderate subgroup (22.0 pg/mL, 95%-CI 16.7–27.4, p = 4.1e–15) and controls (5.8 pg/mL, 95%-CI 4.4–7.3, p = 9.3e–33). Differences remained significant through age 10 (severe: 28.7 pg/mL [95%-CI 25.1–32.4] vs. moderate: 15.7 pg/mL [95%-CI 12.3–19.1], p = 1.0e-6) but converged by age 15 (p = 0.15). Both subgroups (severe: 15.5 pg/mL [95%-CI 12.2–18.9] p = 2.5e-8, moderate: 11.1 pg/mL [95%-CI 6.2–16.1], p = 6.4e-3) remained elevated compared to controls (3.3 pg/mL [95%-CI 1.3–5.3]) until age 15.

Comparison with large, age-matched reference cohorts confirmed the relevance of these elevations[77,78]. Only 1 of 19 samples (5.3%) in the severe subgroup fell within the 99th percentile of age-matched reference values, compared to 2 of 11 samples (18.2%) in the moderate subgroup.

Furthermore, we tested for the association between pNfL levels and SPRS total scores using a linear mixed effects model adjusted for subgroup, age and sex (Figure 6F). While the overall variance in SPRS scores explained by pNfL levels was modest (R_m^2 = 0.12), pNfL

was significantly associated with SPRS (p = 0.013), with each 4.76 pg/mL pNfL increase corresponding to a one-point SPRS increase.

These findings indicate a moderate but consistent, subgroup-dependent elevation of pNfL in early disease stages, particularly pronounced in severe disease trajectories, and detectable in the moderate subgroup before overt acceleration of clinical progression. Given the limited sample size and longitudinal coverage, these observations should be interpreted as exploratory.

Discussion

SPG4 is the most common form of HSP and exhibits marked phenotypic pleiotropy. Although historically framed as a late-onset "pure" HSP, accumulating evidence documents severe early-onset presentations with profound neurodevelopmental impairment and multisystem involvement[47-50]. Prior work has implicated inheritance pattern, genetic anticipation, variant class, and sex as contributors to variability[47-49]; however, as our exploratory analyses confirm, these factors explain only part of the clinical heterogeneity. Advances in understanding spastin biology, particularly its microtubule-severing function[23,64] and the distinct roles of the M1 and M87 isoforms[19], have informed emerging therapeutic strategies[44,54,56,79]. Yet a central challenge remains: as preclinical candidates advance to trials, biologically grounded patient stratification will be essential to detect treatment effects in small cohorts over short follow-up periods typical of trials for rare diseases[57].

We investigated genotype–phenotype correlations in a well-characterized cohort of 206 patients with pathogenic *SPAST* variants, complemented by high-quality literature-derived cases, focusing on individuals under 40 years to capture the window of greatest phenotypic variability and to maximize sensitivity for detecting divergent disease trajectories prior to late-stage convergence.

Longitudinal analyses revealed two distinct clinical trajectories: a subgroup with rapid early progression enriched for missense and *de novo* variants, and a second subgroup with biphasic progression enriched for inherited and truncating variants. However, considerable overlap between clinical and genetic categories indicates that neither inheritance nor variant class alone fully accounts for disease severity. Notably, missense variants showed near-complete segregation by inheritance, consistent with the hypothesis that *de novo* and inherited variants often confer distinct molecular effects on spastin function - an

observation paralleling other neurogenetic disorders in which *de novo* variants are linked to extreme phenotypes and reduced transmission[2,80-83].

Biologically informed stratification framework

To classify missense variants, we adapted the Essential3D framework developed by Iqbal, Brünger, and colleagues[60,61]. Structural mapping revealed that predicted essential residues were enriched at functionally critical sites, including those involved in ATP hydrolysis and microtubule binding, whereas residues at protomer interfaces - expected to impair hexamerization if altered - were not enriched. Extending on the original framework, we introduced a "context-dependent" category for residues with high substitution-specific variability in predicted pathogenicity. This category is exemplified by recurrent variants at Arg499: predicted severe substitutions (p.Arg499His, p.Arg499Leu) associated with earlier onset and rapid progression, whereas predicted moderate substitutions showed later onset; longitudinal data for p.Arg499Cys supported a milder, more slowly progressive course. Based on these findings, we propose a biologically informed patient stratification that integrates essentiality-based missense variant classification with established genotype-phenotype rules to delineate predicted moderate and severe subgroups. We provide comprehensive essentiality predictions for all possible missense variants within residues 318–610 (Table S3), forming the basis for subsequent trajectory analyses and offering practical applicability to clinical stratification.

Divergent disease trajectories

The two identified subgroups exhibited different patterns of disease progression across multiple domains. The severe subgroup exhibited early, severe motor dysfunction with extensive neurodevelopmental impairments including delayed or absent attainment of motor milestones, speech delay, and intellectual disability. Only about a third of patients learned to walk independently, with development stagnating followed by developmental regression. Patients progressed rapidly to wheelchair dependence (median 7.4 years) and near-maximum disability by the second to third decade, with spasticity affecting both lower and upper limbs. This severe presentation was associated with consistently lower and deteriorating health-related quality of life as reported by caregivers.

The moderate subgroup followed a distinctive biphasic course with inflection during the second to third decade. Initially, patients achieved milestones with only modest delays, and maintained motor function (SPRS < 10), and stable quality of life. However, clinical acceleration during adolescence led to progressive functional decline, with patients typically losing the ability to run in the fourth decade and requiring walking aids at a median age of 40 years.

The wide phenotypic spectrum in this subgroup during the initial phase, including subclinical presentations during childhood, likely contributes to under-recognition, delayed diagnosis and bias in retrospectively reported age at onset. Modest but consistent pNfL elevation and slightly delayed milestones in childhood suggest that subclinical disease precedes overt motor impairment by years, consistent with findings from the recent preSPG4 study[76]. Importantly, pNfL is interpreted here as a marker of ongoing axonal injury reflecting disease burden rather than as a validated prognostic or stratification biomarker, given the limited sample size and longitudinal coverage. At the level of directionality, pNfL elevations were concordant with the essentiality-based stratification framework, in that the subgroup predicted to have higher disease burden also exhibited higher pNfL levels in early disease stages. Interpretation of these observations, however, requires consideration of physiological pNfL dynamics during early neurodevelopment. Circulating NfL concentrations are relatively elevated during infancy and early childhood and gradually decline as neurodevelopmental processes stabilize[77,84,85]. Against this background, the elevated pNfL levels observed in the severe subgroup during early disease stages may reflect disease-related axonal injury superimposed on this developmental baseline. Importantly, the reference trajectories shown in Figure 5E correspond to age-dependent physiological pNfL ranges derived from a large previously published pediatric cohort[77,84,85], allowing subgroup trajectories to be interpreted relative to established developmental reference values. Within this context, the observed subgroup differences in early disease stages are consistent with increased axonal injury in the severe trajectory while remaining exploratory given the limited sample size.

For comparisons between subgroups several of the reported effect size estimates were large and accompanied by wide or unbounded confidence intervals. This reflects strong subgroup separation, with some features occurring almost exclusively in one subgroup, as well as low event counts for certain outcomes. Under these conditions, inflated effect sizes and wide confidence intervals are expected despite appropriate penalized or adjusted modeling. Accordingly, these estimates should be interpreted as indicators of substantial relative differences between subgroups rather than precise quantitative risk measures.

Pathomechanistic considerations

Our clinically defined subgroups are broadly consistent with recent experimental results using human neural organoids[55]. In this model, which captures selected aspects of human cortical neuron biology but does not fully recapitulate corticospinal motor neuron identity or circuit-level vulnerability, truncating *SPAST* variants were associated with delayed neurodegeneration compared with a pathogenic missense variant affecting an Essential3D residue. This was accompanied by dysregulation of spastin isoform balance and

subsequent excessive activation of histone deacetylase 6 (HDAC6) mediated via the M1 isoform. While our clinical data do not allow mechanistic inference, these findings are generally compatible with the hypothesis that certain missense variants may precipitate earlier dysregulation of spastin isoform balance, whereas truncating variants may initially permit partial compensation under haploinsufficient conditions.

Limitations

This study has several limitations that merit consideration. First, despite being among the largest systematically characterized SPG4 cohorts, the disorder's rarity and marked phenotypic pleiotropy limited statistical power for some subgroup analyses. Future studies incorporating outcome measures that more specifically quantify developmental, bulbar, upper limb, and autonomic involvement – underappreciated features of severe SPG4 – will enable more robust modeling of additional clinically relevant domains.

A second limitation relates to the multicenter design of the study, which encompassed seven academic centers across four continents and enabled recruitment of a large, deeply phenotyped cohort. However, despite the use of standardized clinical scales and expert assessment, some inter-site variability in the weighting and interpretation of symptoms and clinical scores cannot be fully excluded in the absence of a harmonized prospective assessment protocol or formal inter-site calibration.

Third, the Essential3D framework has several general and gene-specific limitations in the context of SPG4. It relies partly on *in silico* predictions and is constrained by the availability of high-quality structural data, which for spastin currently cover only residues 318–610, precluding assessment of N-terminal variants potentially affecting isoform-specific functions of M1-spastin. In addition, the framework is based on static structural representations and therefore does not capture conformational dynamics. Finally, reliance on variant and population databases introduces potential vulnerability to incompleteness and inaccuracies within these resources.

Finally, while exploration of plasma neurofilament light as a biomarker yielded relevant data extending previous findings[74-76] to the pediatric population, the small sample size, particularly for longitudinal data, does not allow for any definitive conclusions. The present data are insufficient to establish pNfL as a prognostic or stratification biomarker at the individual patient level, and subgroup-dependent differences should be interpreted cautiously. Validation in larger longitudinal cohorts, ideally incorporating additional biomarkers specifically assessing *SPAST*-associated dysregulation[86,87], will be essential.

Given the reverse translational approach that underlies the present study, the proposed stratification framework should be viewed as iterative and subject to refinement. As

additional genotype–phenotype correlations or modifier loci are identified, future iterations may incorporate genetic configurations beyond biallelic *SPAST* variants and missense variants affecting functionally essential residues.

Clinical implications

Despite these limitations, our study provides important insights. First, it offers a biologically grounded stratification framework, informed by protein structure and variant-specific context, that can be applied prospectively once a pathogenic *SPAST* variant is identified. Importantly, this framework is not intended as a deterministic classification system, but rather as a probabilistic tool that integrates variant class, inheritance pattern, and for missense variants Essential3D-based classification – ideally interpreted in the context of genetic precedence – to support early risk stratification without requiring longitudinal clinical data. From a clinical care perspective, early trajectory prediction may support anticipatory guidance. Patients predicted to follow an early severe trajectory may benefit from closer developmental surveillance, earlier multidisciplinary involvement, and proactive assessment of domains that are frequently under-recognized in SPG4, including upper limb, bulbar, and autonomic involvement. Conversely, patients predicted to follow the moderate biphasic trajectory may initially present with subtle or subclinical features; awareness of a later acceleration may reduce diagnostic delay and inform longitudinal monitoring strategies and timely initiation of supportive interventions, including early physiotherapy, which has demonstrated benefit in HSP[88]. From a clinical trial perspective, the framework provides a biologically grounded approach to cohort enrichment and stratified randomization. Grouping patients according to predicted disease trajectory rather than age or variant class alone may reduce phenotypic heterogeneity, improve statistical power to detect treatment effects over shorter follow-up intervals, and inform the selection of therapeutic windows and outcome measures appropriate to subgroup and disease stage.

Moreover, the study delivers the most detailed natural history characterization of SPG4 to date, providing clinically meaningful progression rates, age thresholds across multiple functional domains, and CGI-C-anchored MCID estimates for the SPRS.

Together, these data can support genotype-aware clinical care and facilitate future research efforts through enhanced clinical trial design, stratification, and variant interpretation.

Data availability

Anonymized data and the code supporting the findings of this study are available from the corresponding author upon reasonable request.

Acknowledgements

The authors thank the patients and patients' families for supporting research on SPG4. The contributions of the NIH authors (E.A.Z & A.R.-M.) were made as part of their official duties as NIH federal employees, are in compliance with agency policy requirements, and are considered Works of the United States Government. However, the findings and conclusions presented in this paper are those of the authors and do not necessarily reflect the views of the NIH or the U.S. Department of Health and Human.

Funding

Research in the Ebrahimi-Fakhari Laboratory is supported by the National Institute of Neurological Disorders and Stroke (K08NS123552, 1U54NS148312-01), the Spastic Paraplegia Foundation, the CureAP4 Foundation, the Lilly & Blair Foundation, the CureSPG4 Foundation, the New England Epilepsy Foundation, the Dystonia Medical Research Foundation, the Boston Children's Hospital Translational Research Program, the Boston Children's Hospital TIDO Accelerator Award. V.Q. received a fellowship from the International Parkinson and Movement Disorder Society. L.M.S. received a fellowship from the Deutsche Forschungsgemeinschaft (German Research Foundation, 536105452). D.S. was supported by the Artan Foundation of the University of Zürich. A.R.-M. and E.A.Z were supported by the Intramural Research Program of the National Institute of Neurological Disorders and Stroke and the National Heart, Lung and Blood Institute of the National Institutes of Health (NIH). Research in the Schüle Laboratory is supported by the Federal Ministry of Research, Technology and Space (BMFTR) through funding for the TreatHSP network (grant 01GM2209A), by the European Health and Digital Executive Agency (HADEA) through funding for the European Rare Disease Research Alliance (ERDERA) (grant agreement 101156595) and the MSCA Doctoral Network Medicine Made to Measure (grant agreement #101120256), by the Else Kröner-Fresenius-Stiftung through funding for the Clinician Scientist Programme PRECISE.net, the 'Deutsche Forschungsgemeinschaft' (SCHU 2598/6-1) and the National Institute of Neurological Disorders and Stroke (NINDS)

and the National Institutes of Health (NIH) under Award Number R01NS072248. Several authors are members of the European Reference Network for Rare Neurological Diseases – Project ID 739510 (J.R.R., T.W.R., R.S., L.S.).

Competing interests

Darius Ebrahimi-Fakhari has served as a consultant to Guidepoint LLC and BlackFinBio Ltd. and received speaker honoraria from the Movement Disorder Society, publishing royalties from Cambridge University Press, and reports research funding through a joint research agreement with Astellas Pharmaceuticals Inc and a clinical trial with Neurocrine. The other authors declare no potential conflicts of interest.

Supplementary material

Supplementary material is available at *Brain* online.

References

1. Shribman S, Reid E, Crosby AH, Houlden H, Warner TT. Hereditary spastic paraplegia: from diagnosis to emerging therapeutic approaches. *Lancet Neurol*. Dec 2019;18(12):1136-1146. doi:10.1016/S1474-4422(19)30235-2

2. Alecu JE, Saffari A, Jordan C, Srivastava S, Blackstone C, Ebrahimi-Fakhari D. De novo variants cause complex symptoms in HSP-ATL1 (SPG3A) and uncover genotype-phenotype correlations. *Hum Mol Genet*. Jan 1 2023;32(1):93-103. doi:10.1093/hmg/ddac182

3. Alecu JE, Saffari A, Jumo H, *et al*. Novel CAPN1 missense variants in complex hereditary spastic paraplegia with early-onset psychosis. *Ann Clin Transl Neurol*. Apr 2022;9(4):570-576. doi:10.1002/acn3.51531

4. Coutinho P, Ruano L, Loureiro JL, *et al*. Hereditary ataxia and spastic paraplegia in Portugal: a population-based prevalence study. *JAMA Neurol*. Jun 2013;70(6):746-55. doi:10.1001/jamaneurol.2013.1707

5. Erichsen AK, Koht J, Stray-Pedersen A, Abdelnoor M, Tallaksen CM. Prevalence of hereditary ataxia and spastic paraplegia in southeast Norway: a population-based study. *Brain*. Jun 2009;132(Pt 6):1577-88. doi:10.1093/brain/awp056

6. Ruano L, Melo C, Silva MC, Coutinho P. The global epidemiology of hereditary ataxia and spastic paraplegia: a systematic review of prevalence studies. *Neuroepidemiology*. 2014;42(3):174-83. doi:10.1159/000358801

7. Cao Y, Zheng H, Zhu Z, Yao L, Tian W, Cao L. Clinical and Genetic Spectrum in a Large Cohort of Hereditary Spastic Paraplegia. *Mov Disord*. Apr 2024;39(4):651-662. doi:10.1002/mds.29728

8. Cunha IA, Ribeiro JA, Santos MC. Hereditary spastic paraparesis: The real-world experience from a Neurogenetics outpatient clinic. *Eur J Med Genet*. Mar 2022;65(3):104430. doi:10.1016/j.ejmg.2022.104430

9. Giordani GM, Diniz F, Fussiger H*, et al*. Clinical and molecular characterization of a large cohort of childhood onset hereditary spastic paraplegias. *Sci Rep*. Nov 15 2021;11(1):22248. doi:10.1038/s41598-021-01635-2

10. Schule R, Wiethoff S, Martus P*, et al*. Hereditary spastic paraplegia: Clinicogenetic lessons from 608 patients. *Ann Neurol*. Apr 2016;79(4):646-58. doi:10.1002/ana.24611

11. Yang JO, Yoon JY, Sung DH*, et al*. The emerging genetic diversity of hereditary spastic paraplegia in Korean patients. *Genomics*. Nov 2021;113(6):4136-4148. doi:10.1016/j.ygeno.2021.10.014

12. Yu W, He J, Liu X*, et al*. Clinical features and genetic spectrum of Chinese patients with hereditary spastic paraplegia: A 14-year study. *Front Genet*. 2023;14:1085442. doi:10.3389/fgene.2023.1085442

13. Erfanian Omidvar M, Torkamandi S, Rezaei S*, et al*. Genotype-phenotype associations in hereditary spastic paraplegia: a systematic review and meta-analysis on 13,570 patients. *J Neurol*. Jun 2021;268(6):2065-2082. doi:10.1007/s00415-019-09633-1

14. Dong EL, Wang C, Wu S*, et al*. Clinical spectrum and genetic landscape for hereditary spastic paraplegias in China. *Mol Neurodegener*. Jul 6 2018;13(1):36. doi:10.1186/s13024-018-0269-1

15. Ishiura H, Takahashi Y, Hayashi T*, et al*. Molecular epidemiology and clinical spectrum of hereditary spastic paraplegia in the Japanese population based on comprehensive mutational analyses. *J Hum Genet*. Mar 2014;59(3):163-72. doi:10.1038/jhg.2013.139

16. Mereaux JL, Banneau G, Papin M*, et al*. Clinical and genetic spectra of 1550 index patients with hereditary spastic paraplegia. *Brain*. Apr 29 2022;145(3):1029-1037. doi:10.1093/brain/awab386

17. Boutry M, Morais S, Stevanin G. Update on the Genetics of Spastic Paraplegias. *Curr Neurol Neurosci Rep*. Feb 28 2019;19(4):18. doi:10.1007/s11910-019-0930-2

18. Lo Giudice T, Lombardi F, Santorelli FM, Kawarai T, Orlacchio A. Hereditary spastic paraplegia: clinical-genetic characteristics and evolving molecular mechanisms. *Exp Neurol*. Nov 2014;261:518-39. doi:10.1016/j.expneurol.2014.06.011

19. Ramakrishnan S, Mohan N, Dong Z, Liu M, Qiang L. Unraveling Isoform Complexity: The Roles of M1- and M87-Spastin in Spastic Paraplegia 4 (SPG4). *Mov Disord*. Mar 2025;40(3):420-430. doi:10.1002/mds.30072

20. Claudiani P, Riano E, Errico A, Andolfi G, Rugarli EI. Spastin subcellular localization is regulated through usage of different translation start sites and active export from the nucleus. *Exp Cell Res*. Oct 1 2005;309(2):358-69. doi:10.1016/j.yexcr.2005.06.009

21. Solowska JM, Baas PW. Hereditary spastic paraplegia SPG4: what is known and not known about the disease. *Brain*. Sep 2015;138(Pt 9):2471-84. doi:10.1093/brain/awv178

22. Han H, Schubert HL, McCullough J*, et al*. Structure of spastin bound to a glutamate-rich peptide implies a hand-over-hand mechanism of substrate translocation. *J Biol Chem*. Jan 10 2020;295(2):435-443. doi:10.1074/jbc.AC119.009890

23. Sandate CR, Szyk A, Zehr EA, Lander GC, Roll-Mecak A. An allosteric network in spastin couples multiple activities required for microtubule severing. *Nat Struct Mol Biol*. Aug 2019;26(8):671-678. doi:10.1038/s41594-019-0257-3

24. Roll-Mecak A, Vale RD. Structural basis of microtubule severing by the hereditary spastic paraplegia protein spastin. *Nature*. Jan 17 2008;451(7176):363-7. doi:10.1038/nature06482

25. Solowska JM, Morfini G, Falnikar A*, et al.* Quantitative and functional analyses of spastin in the nervous system: implications for hereditary spastic paraplegia. *J Neurosci*. Feb 27 2008;28(9):2147-57. doi:10.1523/JNEUROSCI.3159-07.2008

26. Evans KJ, Gomes ER, Reisenweber SM, Gundersen GG, Lauring BP. Linking axonal degeneration to microtubule remodeling by Spastin-mediated microtubule severing. *J Cell Biol*. Feb 14 2005;168(4):599-606. doi:10.1083/jcb.200409058

27. Roll-Mecak A, Vale RD. The Drosophila homologue of the hereditary spastic paraplegia protein, spastin, severs and disassembles microtubules. *Curr Biol*. Apr 12 2005;15(7):650-5. doi:10.1016/j.cub.2005.02.029

28. Kuo YW, Trottier O, Mahamdeh M, Howard J. Spastin is a dual-function enzyme that severs microtubules and promotes their regrowth to increase the number and mass of microtubules. *Proc Natl Acad Sci U S A*. Mar 19 2019;116(12):5533-5541. doi:10.1073/pnas.1818824116

29. Vemu A, Szczesna E, Zehr EA*, et al*. Severing enzymes amplify microtubule arrays through lattice GTP-tubulin incorporation. *Science*. Aug 24 2018;361(6404)doi:10.1126/science.aau1504

30. Valenstein ML, Roll-Mecak A. Graded Control of Microtubule Severing by Tubulin Glutamylation. *Cell*. Feb 25 2016;164(5):911-21. doi:10.1016/j.cell.2016.01.019

31. Stone MC, Rao K, Gheres KW*, et al*. Normal spastin gene dosage is specifically required for axon regeneration. *Cell Rep*. Nov 29 2012;2(5):1340-50. doi:10.1016/j.celrep.2012.09.032

32. Aiken J, Holzbaur ELF. Spastin locally amplifies microtubule dynamics to pattern the axon for presynaptic cargo delivery. *Curr Biol*. Apr 22 2024;34(8):1687-1704 e8. doi:10.1016/j.cub.2024.03.010

33. Brill MS, Kleele T, Ruschkies L*, et al*. Branch-Specific Microtubule Destabilization Mediates Axon Branch Loss during Neuromuscular Synapse Elimination. *Neuron*. Nov 23 2016;92(4):845-856. doi:10.1016/j.neuron.2016.09.049

34. Butler R, Wood JD, Landers JA, Cunliffe VT. Genetic and chemical modulation of spastin-dependent axon outgrowth in zebrafish embryos indicates a role for impaired microtubule dynamics in hereditary spastic paraplegia. *Dis Model Mech*. Nov-Dec 2010;3(11-12):743-51. doi:10.1242/dmm.004002

35. Costa AC, Sousa MM. The Role of Spastin in Axon Biology. *Front Cell Dev Biol*. 2022;10:934522. doi:10.3389/fcell.2022.934522

36. Wood JD, Landers JA, Bingley M*, et al*. The microtubule-severing protein Spastin is essential for axon outgrowth in the zebrafish embryo. *Hum Mol Genet*. Sep 15 2006;15(18):2763-71. doi:10.1093/hmg/ddl212

37. Arribat Y, Grepper D, Lagarrigue S, Qi T, Cohen S, Amati F. Spastin mutations impair coordination between lipid droplet dispersion and reticulum. *PLoS Genet*. Apr 2020;16(4):e1008665. doi:10.1371/journal.pgen.1008665

38. Chang CL, Weigel AV, Ioannou MS*, et al*. Spastin tethers lipid droplets to peroxisomes and directs fatty acid trafficking through ESCRT-III. *J Cell Biol*. Aug 5 2019;218(8):2583-2599. doi:10.1083/jcb.201902061

39. Papadopoulos C, Orso G, Mancuso G*, et al*. Spastin binds to lipid droplets and affects lipid metabolism. *PLoS Genet*. Apr 2015;11(4):e1005149. doi:10.1371/journal.pgen.1005149

40. Park SH, Zhu PP, Parker RL, Blackstone C. Hereditary spastic paraplegia proteins REEP1, spastin, and atlastin-1 coordinate microtubule interactions with the tubular ER network. *J Clin Invest*. Apr 2010;120(4):1097-110. doi:10.1172/JCI40979

41. Rizo T, Gebhardt L, Riedlberger J*, et al*. Store-operated calcium entry is reduced in spastin-linked hereditary spastic paraplegia. *Brain*. Sep 14 2022;145(9):3131-3146. doi:10.1093/brain/awac122

42. Cai Z, Wu H, Jiang T*, et al*. The Cullin3-Ring E3 ubiquitin ligase complex and USP14 regulate spastin-mediated microtubule severing and promotion of neurite outgrowth. *Neural Regen Res*. Apr 1 2026;21(4):1641-1651. doi:10.4103/NRR.NRR-D-25-00037

43. Kang HM, Kim DH, Kim M*, et al*. FBXL17/spastin axis as a novel therapeutic target of hereditary spastic paraplegia. *Cell Biosci*. Jul 22 2022;12(1):110. doi:10.1186/s13578-022-00851-1

44. Sardina F, Carsetti C, Giorgini L, Fattorini G, Cestra G, Rinaldo C. Cul-4 inhibition rescues spastin levels and reduces defects in hereditary spastic paraplegia models. *Brain*. Oct 3 2024;147(10):3534-3546. doi:10.1093/brain/awae095

45. Harding AE. Classification of the hereditary ataxias and paraplegias. *Lancet*. May 21 1983;1(8334):1151-5. doi:10.1016/s0140-6736(83)92879-9

46. de Bot ST, van den Elzen RT, Mensenkamp AR, *et al*. Hereditary spastic paraplegia due to SPAST mutations in 151 Dutch patients: new clinical aspects and 27 novel mutations. *J Neurol Neurosurg Psychiatry*. Oct 2010;81(10):1073-8. doi:10.1136/jnnp.2009.201103

47. Mo A, Saffari A, Kellner M, *et al*. Early-Onset and Severe Complex Hereditary Spastic Paraplegia Caused by De Novo Variants in SPAST. *Mov Disord*. Dec 2022;37(12):2440-2446. doi:10.1002/mds.29225

48. Parodi L, Fenu S, Barbier M, *et al*. Spastic paraplegia due to SPAST mutations is modified by the underlying mutation and sex. *Brain*. Dec 1 2018;141(12):3331-3342. doi:10.1093/brain/awy285

49. Schieving JH, de Bot ST, van de Pol LA, *et al*. De novo SPAST mutations may cause a complex SPG4 phenotype. *Brain*. Jul 1 2019;142(7):e31. doi:10.1093/brain/awz140

50. Varghaei P, Estiar MA, Ashtiani S, *et al*. Genetic, structural and clinical analysis of spastic paraplegia 4. *Parkinsonism Relat Disord*. May 2022;98:62-69. doi:10.1016/j.parkreldis.2022.03.019

51. Chelban V, Tucci A, Lynch DS, *et al*. Truncating mutations in SPAST patients are associated with a high rate of psychiatric comorbidities in hereditary spastic paraplegia. *J Neurol Neurosurg Psychiatry*. Aug 2017;88(8):681-687. doi:10.1136/jnnp-2017-315796

52. Degoutin M, Angelini C, Bar C, *et al*. From spastic paraplegia to infantile neurodegenerative disorder: Expanding the phenotypic spectrum associated with biallelic SPAST variants. *Eur J Neurol*. Jan 2025;32(1):e70025. doi:10.1111/ene.70025

53. Nolasco GA, Roldan M, Jamshidi Y, *et al*. Expanding Hereditary Spastic Paraplegias Limits: Biallelic SPAST Variants in Cerebral Palsy Mimics. *Ann Clin Transl Neurol*. Sep 26 2025;doi:10.1002/acn3.70206

54. Havlicek S, Kohl Z, Mishra HK, *et al*. Gene dosage-dependent rescue of HSP neurite defects in SPG4 patients' neurons. *Hum Mol Genet*. May 15 2014;23(10):2527-41. doi:10.1093/hmg/ddt644

55. Mohan N, Ramakrishnan S, Sun X, *et al*. Genotype-Phenotype Distinctions in Spastic Paraplegia 4 Reveal HDAC6 as a Therapeutic Target. *bioRxiv*. Jul 18 2025;doi:10.1101/2025.07.15.664947

56. Nakazeki F, Tsuge I, Horie T, *et al*. MiR-33a is a therapeutic target in SPG4-related hereditary spastic paraplegia human neurons. *Clin Sci (Lond)*. Feb 28 2019;133(4):583-595. doi:10.1042/CS20180980

57. Pizzamiglio C, Vernon HJ, Hanna MG, Pitceathly RDS. Designing clinical trials for rare diseases: unique challenges and opportunities. *Nat Rev Methods Primers*. Dec 2022;2(1)doi:10.1038/s43586-022-00100-2

58. Schule R, Holland-Letz T, Klimpe S, *et al*. The Spastic Paraplegia Rating Scale (SPRS): a reliable and valid measure of disease severity. *Neurology*. Aug 8 2006;67(3):430-4. doi:10.1212/01.wnl.0000228242.53336.90

59. Svenstrup K, Bross P, Koefoed P, *et al*. Sequence variants in SPAST, SPG3A and HSPD1 in hereditary spastic paraplegia. *J Neurol Sci*. Sep 15 2009;284(1-2):90-5. doi:10.1016/j.jns.2009.04.024

60. Iqbal S, Brunger T, Perez-Palma E, *et al*. Delineation of functionally essential protein regions for 242 neurodevelopmental genes. *Brain*. Feb 13 2023;146(2):519-533. doi:10.1093/brain/awac381

61. Iqbal S, Perez-Palma E, Jespersen JB, *et al*. Comprehensive characterization of amino acid positions in protein structures reveals molecular effect of missense variants. *Proc Natl Acad Sci U S A*. Nov 10 2020;117(45):28201-28211. doi:10.1073/pnas.2002660117

62. Alecu JE, Saffari A, Ziegler M, *et al*. Plasma Neurofilament Light Chain Is Elevated in Adaptor Protein Complex 4-Related Hereditary Spastic Paraplegia. *Mov Disord*. Sep 2023;38(9):1742-1750. doi:10.1002/mds.29524

63. Zehr E, Szyk A, Piszczek G, Szczesna E, Zuo X, Roll-Mecak A. Katanin spiral and ring structures shed light on power stroke for microtubule severing. *Nat Struct Mol Biol*. Sep 2017;24(9):717-725. doi:10.1038/nsmb.3448

64. Eckert T, Link S, Le DT, *et al*. Subunit Interactions and cooperativity in the microtubule-severing AAA ATPase spastin. *J Biol Chem*. Jul 27 2012;287(31):26278-90. doi:10.1074/jbc.M111.291898

65. Fan X, Lin Z, Fan G, *et al*. The AAA protein spastin possesses two levels of basal ATPase activity. *FEBS Lett*. May 2018;592(10):1625-1633. doi:10.1002/1873-3468.13075

66. Wen M, Wang C. The nucleotide cycle of spastin correlates with its microtubule-binding properties. *FEBS J*. Aug 2013;280(16):3868-77. doi:10.1111/febs.12385

67. Gillespie MK, Humphreys P, McMillan HJ, Boycott KM. Association of Early-Onset Spasticity and Risk for Cognitive Impairment With Mutations at Amino Acid 499 in SPAST. *J Child Neurol*. Apr 2018;33(5):329-332. doi:10.1177/0883073818756680

68. Nan H, Shiraku H, Mizuno T, Takiyama Y. A p.Arg499His mutation in SPAST is associated with infantile-onset complicated spastic paraplegia: a case report and review of the literature. *BMC Neurol*. Nov 9 2021;21(1):439. doi:10.1186/s12883-021-02478-0

69. Ogasawara M, Saito T, Koshimizu E, Akasaka N, Sasaki M. A p.Arg499His Mutation in SPAST Is Associated with Infantile Onset Ascending Spastic Paralysis Complicated with Dysarthria and Anarthria. *Neuropediatrics*. Dec 2019;50(6):391-394. doi:10.1055/s-0039-1694973

70. Ribai P, Depienne C, Fedirko E, *et al*. Mental deficiency in three families with SPG4 spastic paraplegia. *Eur J Hum Genet*. Jan 2008;16(1):97-104. doi:10.1038/sj.ejhg.5201922

71. Xu L, Peng Z, Zhou C, *et al*. A Chinese Patient with Spastic Paraplegia Type 4 with a De Novo Mutation in the SPAST Gene. *Case Rep Genet*. 2021;2021:6636855. doi:10.1155/2021/6636855

72. Parodi L, Barbier M, Jacoupy M, *et al*. The mitochondrial seryl-tRNA synthetase SARS2 modifies onset in spastic paraplegia type 4. *Genet Med*. Nov 2022;24(11):2308-2317. doi:10.1016/j.gim.2022.07.023

73. Narayanan UG, Fehlings D, Weir S, Knights S, Kiran S, Campbell K. Initial development and validation of the Caregiver Priorities and Child Health Index of Life with Disabilities (CPCHILD). *Dev Med Child Neurol*. Oct 2006;48(10):804-12. doi:10.1017/S0012162206001745

74. Kessler C, Ruschil C, Abdelhak A, *et al*. Serum Neurofilament Light Chain and Glial Fibrillary Acidic Protein as Biomarkers in Primary Progressive Multiple Sclerosis and Hereditary Spastic Paraplegia Type 4. *Int J Mol Sci*. Nov 3 2022;23(21)doi:10.3390/ijms232113466

75. Kessler C, Serna-Higuita LM, Wilke C, *et al*. Characteristics of serum neurofilament light chain as a biomarker in hereditary spastic paraplegia type 4. *Ann Clin Transl Neurol*. Mar 2022;9(3):326-338. doi:10.1002/acn3.51518

76. Rattay TW, Volker M, Rautenberg M, *et al*. The prodromal phase of hereditary spastic paraplegia type 4: the preSPG4 cohort study. *Brain*. Mar 1 2023;146(3):1093-1102. doi:10.1093/brain/awac155

77. Abdelhak A, Petermeier F, Benkert P, *et al*. Serum neurofilament light chain reference database for individual application in paediatric care: a retrospective modelling and validation study. *Lancet Neurol*. Sep 2023;22(9):826-833. doi:10.1016/S1474-4422(23)00210-7

78. Benkert P, Meier S, Schaedelin S, *et al*. Serum neurofilament light chain for individual prognostication of disease activity in people with multiple sclerosis: a retrospective modelling and validation study. *Lancet Neurol*. Mar 2022;21(3):246-257. doi:10.1016/S1474-4422(22)00009-6

79. Mohan N, Qiang L, Morfini G, Baas PW. Therapeutic Strategies for Mutant SPAST-Based Hereditary Spastic Paraplegia. *Brain Sci*. Aug 18 2021;11(8)doi:10.3390/brainsci11081081

80. Acuna-Hidalgo R, Veltman JA, Hoischen A. New insights into the generation and role of de novo mutations in health and disease. *Genome Biol*. Nov 28 2016;17(1):241. doi:10.1186/s13059-016-1110-1

81. Coe BP, Stessman HAF, Sulovari A, *et al*. Neurodevelopmental disease genes implicated by de novo mutation and copy number variation morbidity. *Nat Genet*. Jan 2019;51(1):106-116. doi:10.1038/s41588-018-0288-4

82. Erickson RP. The importance of de novo mutations for pediatric neurological disease--It is not all in utero or birth trauma. *Mutat Res Rev Mutat Res*. Jan-Mar 2016;767:42-58. doi:10.1016/j.mrrev.2015.12.002

83. Wilfert AB, Sulovari A, Turner TN, Coe BP, Eichler EE. Recurrent de novo mutations in neurodevelopmental disorders: properties and clinical implications. *Genome Med*. Nov 27 2017;9(1):101. doi:10.1186/s13073-017-0498-x

84. Geis T, Gutzeit S, Fouzas S, *et al*. Serum Neurofilament light chain (NfL) levels in children with and without neurologic diseases. *Eur J Paediatr Neurol*. Jul 2023;45:9-13. doi:10.1016/j.ejpn.2023.05.003

85. Stukas S, Cooper J, Higgins V, Holmes D, Adeli K, Wellington CL. Pediatric reference intervals for serum neurofilament light and glial fibrillary acidic protein using the Canadian Laboratory Initiative on Pediatric Reference Intervals (CALIPER) cohort. *Clin Chem Lab Med*. Mar 25 2024;62(4):698-705. doi:10.1515/cclm-2023-0660

86. Sardina F, Valente D, Fattorini G, *et al*. New cellular imaging-based method to distinguish the SPG4 subtype of hereditary spastic paraplegia. *Eur J Neurol*. Jun 2023;30(6):1734-1744. doi:10.1111/ene.15756

87. Wali G, Siow SF, Liyanage E, Kumar KR, Mackay-Sim A, Sue CM. Reduced acetylated alpha-tubulin in SPAST hereditary spastic paraplegia patient PBMCs. *Front Neurosci*. 2023;17:1073516. doi:10.3389/fnins.2023.1073516

88. Di Ludovico A, Ciarelli F, La Bella S, Scorrano G, Chiarelli F, Farello G. The therapeutic effects of physical treatment for patients with hereditary spastic paraplegia: a narrative review. *Front Neurol*. 2023;14:1292527. doi:10.3389/fneur.2023.1292527

Figure legends

Figure 1 Genetic spectrum and essentiality mapping of spastin residues. (**A**) Genetic spectrum of the cohort with inner track representing proportions of inheritance patterns and outer track representing coding impacts, with proportions nested within the respective mode of inheritance. (**B**) Pathogenic variants identified in the cohort, annotated along the M1-spastin primary structure. Protein-truncating variants are depicted toward the top and nontruncating variants downward. (**C**) SPRS scores in the combined literature- and study-derived dataset. Longitudinal observations from the same patient are connected by lines. (**D**) Venn diagram depicting overlaps of distinct missense variants according to inheritance pattern in the combined dataset. (**E**) Schematic of the modified Essential3D classification approach. (**F**) *Top*: Heatmap depicting variables used for essentiality mapping, including distribution of essentiality categories. *Bottom*: human wildtype spastin hexamer structure (PDB: 6PEN) with residues colored by essentiality verdict.

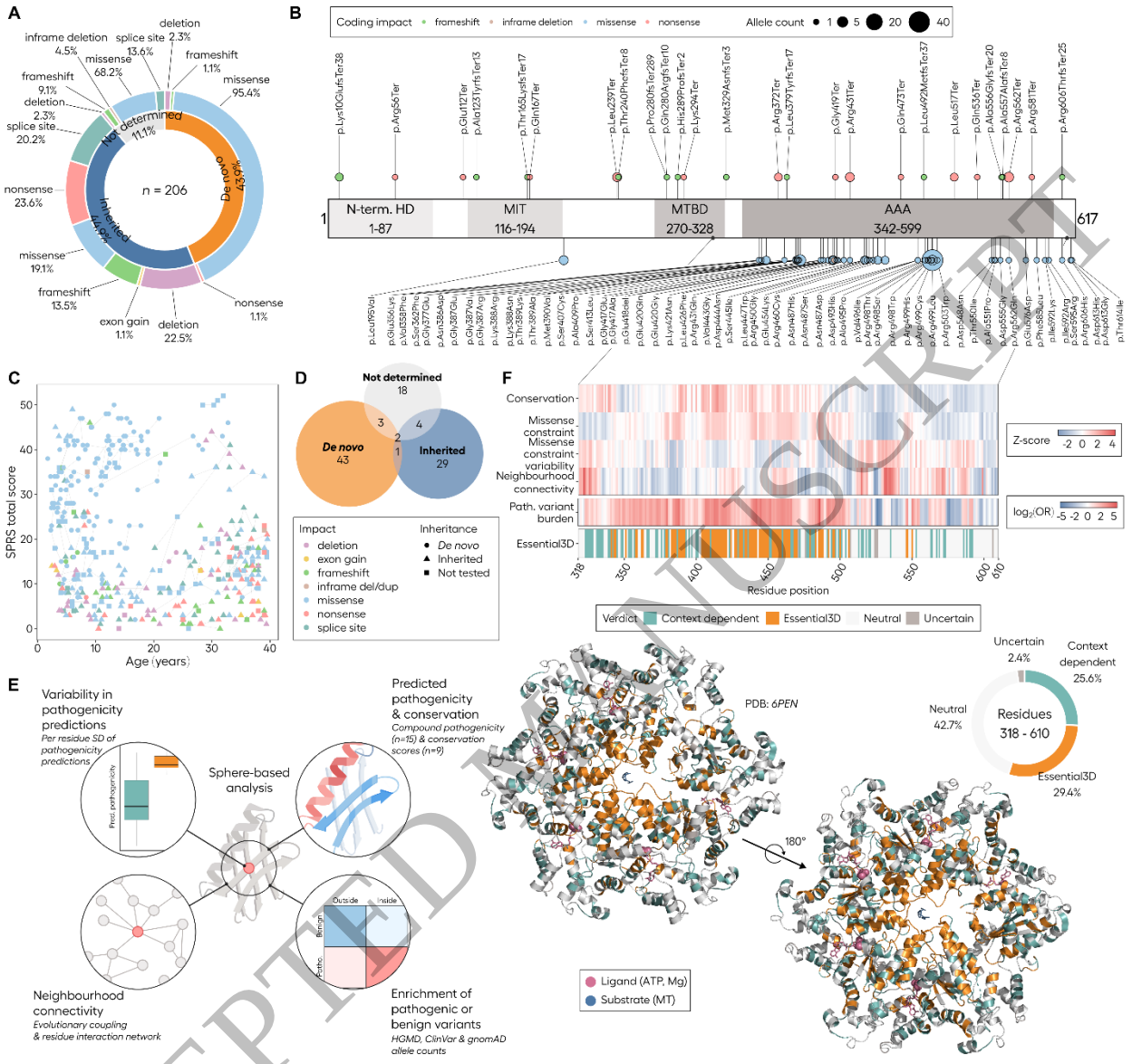

Figure 2 Arg499 exemplifies context-dependent essentiality. (**A**) Enrichment analysis of structural and functional features across essentiality verdicts. Black circles surrounding dots indicate $p_{adj.} < 0.05$. (**B**) Zoom-in view on the Arg499 residue neighborhood with residues colored according to essentiality verdict. Ligands (ATP, BeF, and Mg^{2+}) shown in purple. (**C**) Pathogenicity predictions for Arg499 amino acid substitutions. For subclassification into moderate and severe variants, pathogenicity scores were Z-transformed for each residue separately. (**D**) SPRS scores in patients with Arg499 variants in the combined dataset. Longitudinal observations from the same patient are connected by lines. (**E**) Age at onset comparison between Arg499 missense variants. Kruskal-Wallis, p = 2.6e-10; p values of pairwise comparisons shown, using Dunn's post-hoc test; d

represents Cohen's d. Box-and-whisker plots display the median (center line), interquartile range (box), and minimum and maximum values (whiskers).

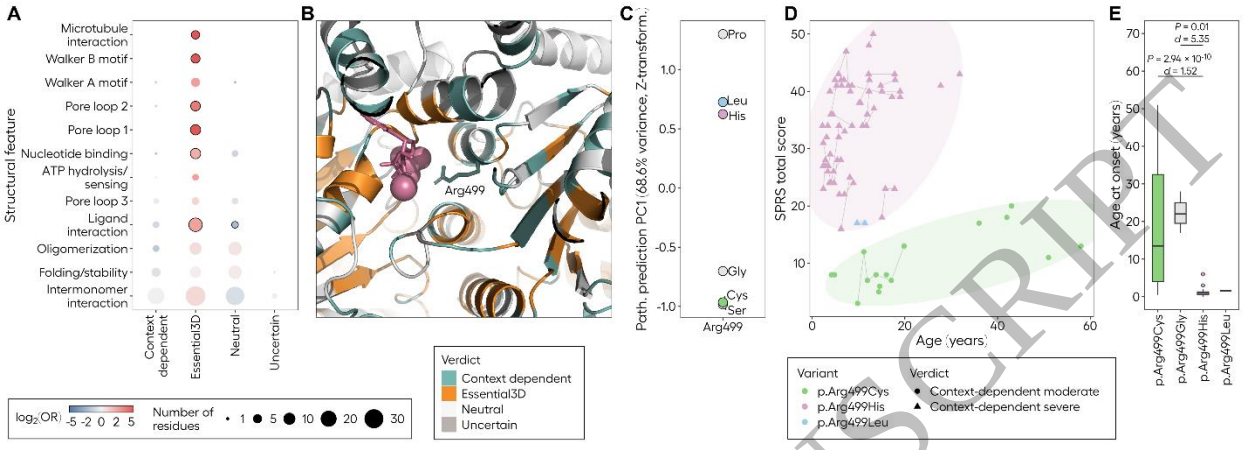

Figure 3 Stratification framework, quality of life and phenotypic spectra. (**A**) Comparison of reported ages at onset in the combined dataset stratified by essentiality verdict, excluding uncertain classifications. Main plot: Kruskal-Wallis, p < 1e-16, p values of pairwise comparisons shown, using Dunn's post-hoc test; subplot: Mann-Whitney U test; d represents Cohen's d. Half violin and box plots show the distribution of the data as a kernel density estimate on the left and a box-and-whisker summary on the right, indicating the median (center line), interquartile range (box), and minimum and maximum values (whiskers). (**B**) Schematic of the proposed stratification framework. (**C**) Interaction plot, with dots representing estimated marginal means (EMM) at selected timepoints (3, 5, 10, 13.7, 20, 25, 30 years). Vertical ribbons indicating EMM 95%-CIs. Top row p values for cross-sectional EMM contrasts at selected timepoints. (**D**) Separate subgroup models with kernel density estimates. Longitudinal observations from the same patient are connected by lines. (**E**) Results from phenotypic enrichment analysis using Firth's logistic regression. Labelled dots represent clinical findings that were nominally enriched, and black circles surrounding dots indicate q < 0.05. (**F**) Frequency of extrapyramidal movement disorders stratified by subgroup.

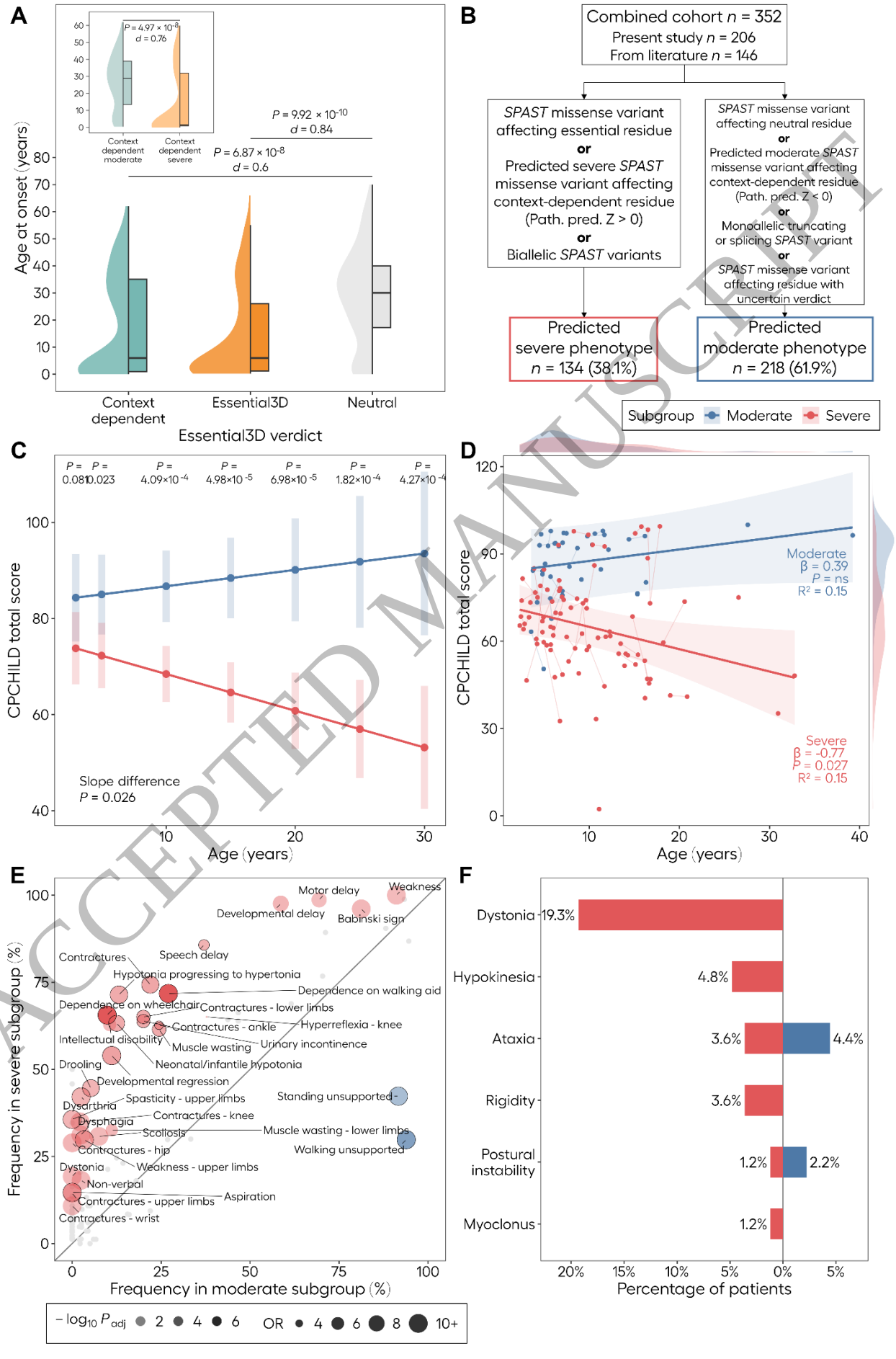

Figure 4 Divergent functional motor impairments between subgroups. Kaplan-Meier estimators for SPATAX disability stages in the moderate (**A**) and severe (**B**) subgroup. 95%-CIs are shown as shaded ribbons. (**C**) Association between SPATAX and CPCHILD. Linear-mixed effects model adjusted for subgroup, age, and sex. Longitudinal observations from the same patient are connected by lines. (**D** & **E**) Kaplan-Meier estimators for GMFCS scores in the moderate (**D**) and severe (**E**) subgroup. 95%-CIs are shown as shaded ribbons. (**F**) Association between GMFCS and CPCHILD. Linear-mixed effects model adjusted for subgroup, age, and sex. Longitudinal observations from the same patient are connected by lines. (**G**, **H** & **I**) Covariate-adjusted survival curves derived from Cox proportional hazards models for SPATAX threshold severe gait impairment, requiring unilateral support (≥4) (G) and wheelchair dependence (≥6) (H) and GMFCS threshold ≥III (requiring assistive mobility device) (I). Covariates included subgroup, sex, and inheritance pattern.

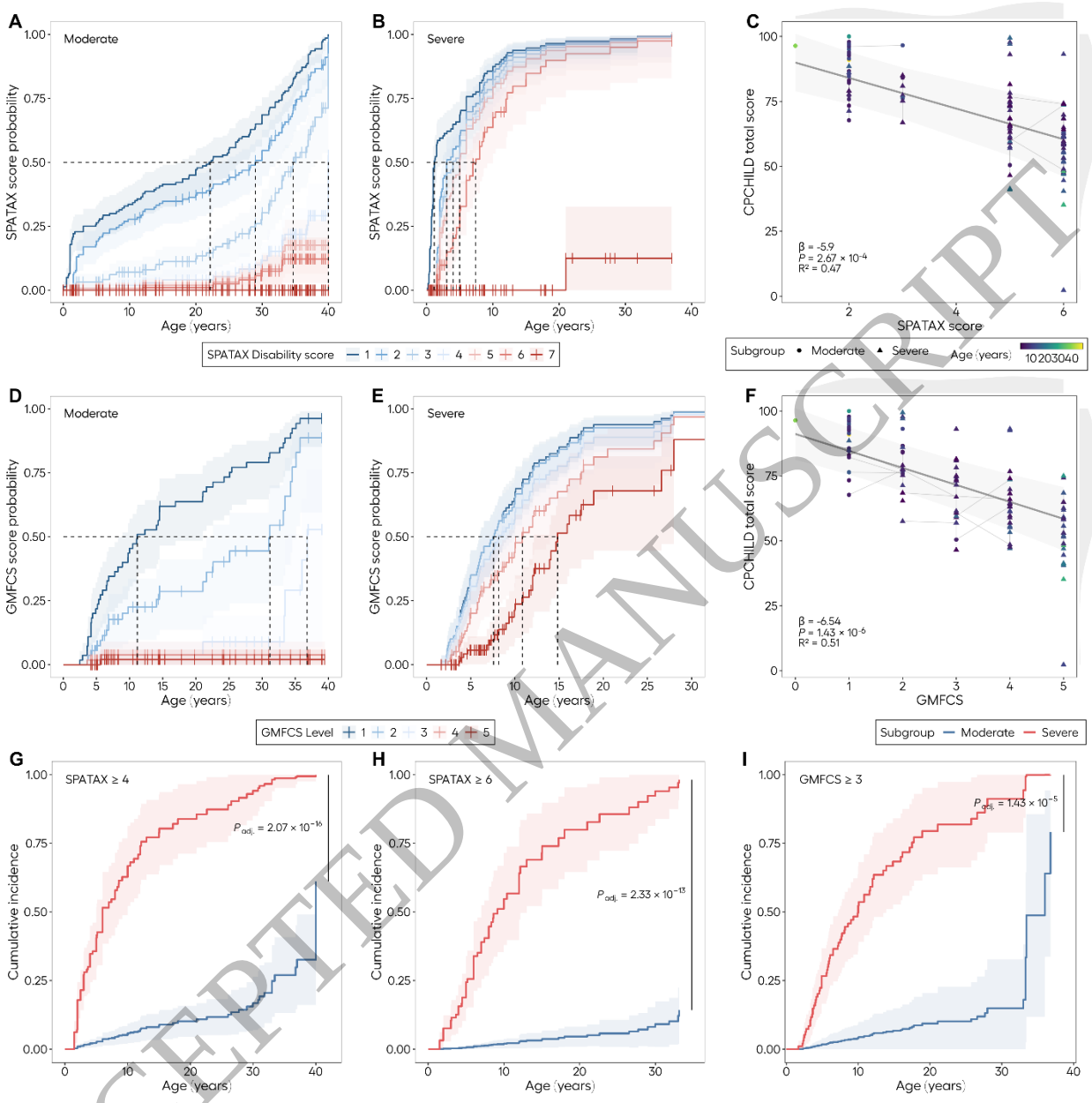

Figure 5 Differential progression of spasticity between subgroups. (**A**) Interaction plot for segmented linear mixed-effects regression of the SPRS total score, with dots representing EMM at selected timepoints (3, 5, 10, 13.7, 20, 25, 30 years). Vertical ribbons indicating EMM 95%-CIs. Top row p values for cross-sectional EMM contrasts at selected timepoints. Gray vertical ribbon indicates estimated breakpoint for the moderate subgroup. (**B**) Separate subgroup models for SPRS total scores with kernel density estimates. (**C**) Association between SPRS total score and CPCHILD. Linear-mixed effects model adjusted for subgroup, age, and sex. (**D**) Interaction plot for linear mixed-effects regression of the SPRS spasticity subscore (SPRS items 7-10), with dots representing EMM at selected timepoints (3, 5, 10, 13.7, 20, 25, 30 years). Vertical ribbons indicating EMM 95%-CIs. Top

row p values for cross-sectional EMM contrasts at selected timepoints. (**E**) Separate subgroup models for SPRS spasticity subscores with kernel density estimates. (**F**) Association between SPRS spasticity subscore and CPCHILD. Linear-mixed effects model adjusted for subgroup, age, and sex. (**G** & **H**) Ordinal generalized additive mixed-effects models for modified Ashworth scale values stratified by lower (G) and upper (H) limb muscle groups in the severe subgroup. Shaded ribbons indicate 95% CIs. (**I**) MCID estimations estimates for SPRS total scores stratified by CGI-C anchor definition. Bars representing SPRS change EMM derived from a linear-mixed-effects model adjusting for baseline SPRS, age at anchor assessment, interval between visits, subgroup and sex as covariates. Vertical lines indicate EMM 95% CIs. (B, C, E & F) Longitudinal observations from the same patient are connected by lines.

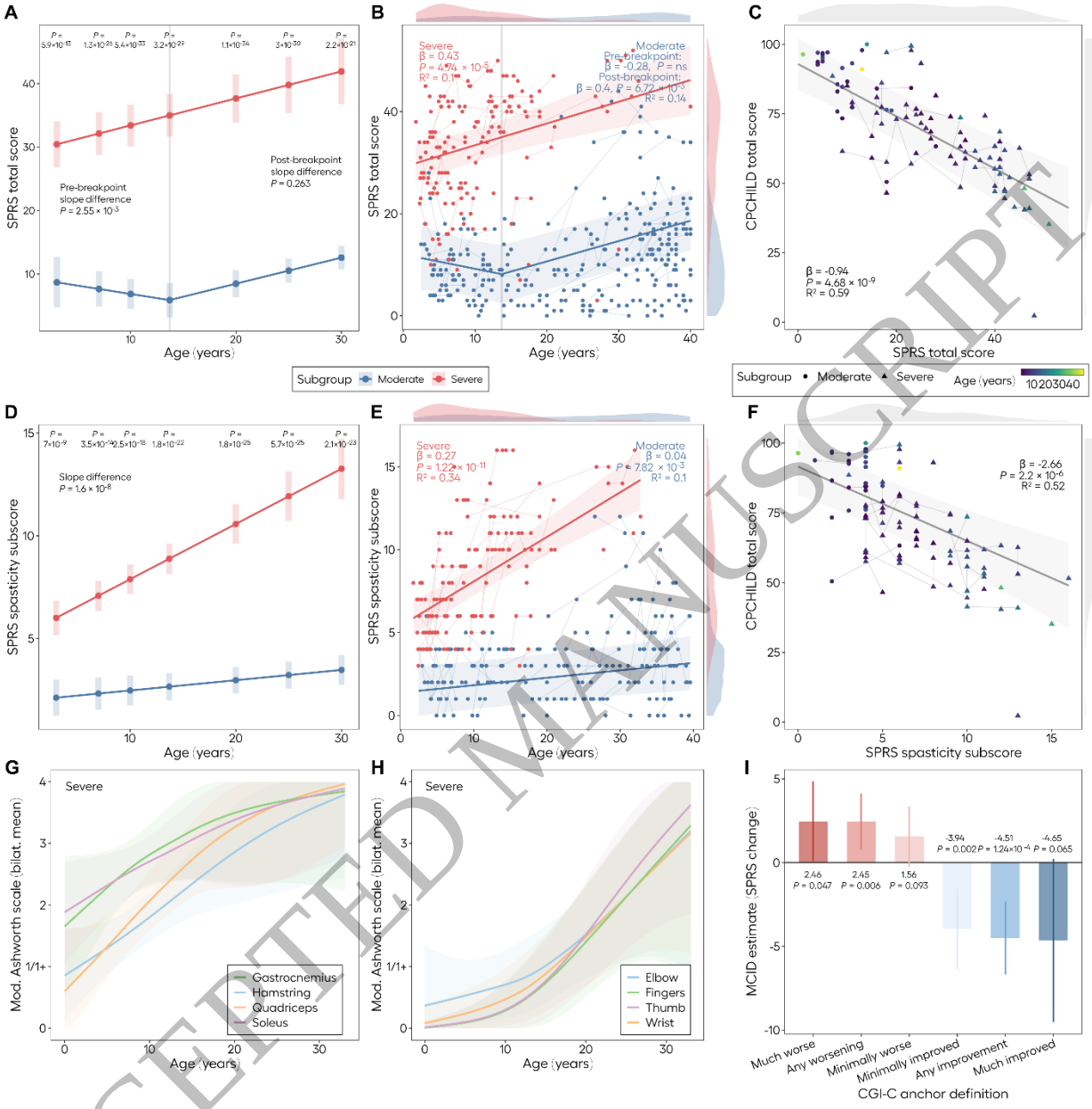

Figure 6 Developmental trajectories and plasma NfL. (**A**) Kaplan-Meier estimators for time-to-milestone attainment in the severe subgroup. Shaded ribbons indicate 95% CIs. (**B** & **C**) Kaplan-Meier estimators for time-to-unsupported standing (B) and time-to-unsupported walking (C) stratified by subgroup. Curves were compared using log-rank test. (**D**) Generalized additive mixed-effects modeling of developmental quotients stratified by domain in the severe subgroup. Shaded ribbons indicate 95% CIs. (**E**) Plasma NfL over time stratified by subgroup with kernel density estimates. Dotted lines indicate 1st and 99th percentile of pNfL reference models in healthy individuals derived from previously published studies. (**F**) Association between pNfL and SPRS total scores. Linear-mixed

effects model adjusted for subgroup, age, and sex. (E & F) Longitudinal observations from the same patient are connected by lines.